Applied Surface Science 427 (2018) 357–362

Contents lists available at ScienceDirect

Applied Surface Science

journal homepage: www.elsevier.com/locate/apsusc

Full Length Article

A DFT based method for calculating the surface energies of asymmetric MoP facets

Xinxin Tian[a,*], Tao Wang[b,*], Lifang Fan[c], Yuekui Wang[a], Haigang Lu[a], Yuewen Mu[a]

[a] Institute of Molecular Science, Key Laboratory of Materials for Energy Conversion and Storage of Shanxi Province, Shanxi University, Taiyuan 030006, China
[b] Univ Lyon, Ens de Lyon, CNRS UMR 5182, Université Claude Bernard Lyon 1, Laboratoire de Chimie, F69342, Lyon, France
[c] Institute of Environmental Science, Shanxi University, Taiyuan 030006, China

ARTICLE INFO

Article history:
Received 8 July 2017
Received in revised form 4 August 2017
Accepted 25 August 2017
Available online 1 September 2017

Keywords:
MoP
Asymmetric surface
Surface stability
Morphology
DFT

ABSTRACT

MoP is a promising catalyst in heterogeneous catalysis. Understanding its surface stability and morphology is the first and essential step in exploring its catalytic properties. However, traditional surface energy calculation method does not work for the asymmetric termination of MoP. In this work, we reported a useful DFT based method to get the surface energies of asymmetric MoP facets. Under ideal condition, the (101) surface with mixed Mo/P termination is most stable, followed by the (100) surface, while the (001) surface is least stable. Wulff construction reveals the exposure of six surfaces on the MoP nanoparticle, where the (101) has the largest contribution. Atomistic thermodynamics results reveal the changes in surface stability orders with experimental conditions, and the (001)-P termination becomes more and more stable with increasing P chemical potential, which indicates its exposure is possible at defined conditions. Our results agree well with the previous experimental XRD and TEM data. We believe the reported method for surface energy calculation could be extended to other similar systems with asymmetric surface terminations.

1. Introduction

Catalysis is becoming more and more essential in modern chemistry and energy society, and the catalysts with low cost, high activity and selectivity as well as high resistance to contamination are possible and suitable for industry applications. Molybdenum based catalysts like Mo_2C, MoS_2 and MoP composed a group of promising candidates with these advantages. It is reported that they have excellent activities in many processes, such as syngas conversion to hydrocarbon or oxygenated chemicals [1], biorefinery [2,3], and advanced hydroprocessing [4]. Among these molybdenum catalysts, MoP has attracted great attentions from the fields of hydrogen evolution reaction (HER) [5–7], hydrogen oxidation reaction (HOR) [8], hydrodenitrogenation (HDN) [9], hydrodesulfurization (HDS) [10], hydrodeoxygenation (HDO) [11], hydrodechlorination (HDC) [12], hydroisomerization [13], photocatalytic hydrogen production [14] as well as anode materials for lithium-ion batteries [15]. However, the most interesting property of MoP is the high activity and selectivity in alcohol synthesis [16,17], especially when it is promoted by the alkali metals and/or Group VIII metals.

Theoretically, there are very limited available results about the catalytic properties of MoP. For the CO hydrogenation reaction, Feng et al. [18] and Liu et al. [19] found that CO adsorption on the Mo atop site is most favored on MoP(001) surface. Zaman et al. [20–23] investigated CO and H_2 adsorption as well as dissociation on the MoP(001) and MoP (100) surfaces, where the Mo atop was also found to be the most favorable site for both CO and H_2 adsorption. Moreover, these two surfaces were proved to have very low activity in CO dissociation. However, H_2 dissociation on MoP(100) surface was more favored than MoP(001) surface, and they finally identified the MoP(100) surface as the active plane for CO hydrogenation reaction. For the HDN and HDS reactions, Milman et al. [24] studied the adsorption of o-propylaniline and subsequent C—N hydrogenolysis into propylbenzene. It is found that the weaken of C—N and aromatic C—C bonds is responsible for the high HDN activity of MoP. Li et al. [25] investigated the initial hydrogenations of pyridine on MoP(001) surface and checked different potential hydrogen sources, where the surface H atoms was identified as the most rational one followed by adsorbed H_2S and SH. Deng et al. [26] calculated the HDN mechanism of pyridine on MoP(010) surface and the side-on adsorption mode of pyridine was found to

* Corresponding authors.
E-mail addresses: tianxx@sxu.edu.cn (X. Tian), tao.wang@ens-lyon.fr (T. Wang).

http://dx.doi.org/10.1016/j.apsusc.2017.08.172
0169-4332/

be most stable. It was also found that the denitrification process could only be competitive after the fourth hydrogenation step of 1,3,4,5-Tetrahydropyridine. Li et al.[27] studied the adsorption and C—N bond cleavage mechanism of aniline on MoP(001) surface and found that aniline preferred the flat adsorption configuration, and the direct C—N bond cleavage proceeded mainly via deamination with co-adsorbed H_2 to produce benzene and ammonia. Ren et al. [28] found that thiophene adsorbed dissociatively on MoP(001) surface but nondissociatively on γ-Mo_2N(100) and Ni_2P(001) surfaces. More recently, Fields et al. [29] reported the scaling relation for the hydrogenated C, N and O species on a variety of doped P-terminated MoP surfaces, and suggested that phosphorus experiences a shift in preferred bond order depending on the degree of hydrogen substitution on the adsorbate. This shift in phosphorus hybridization could result in selective bond weakening or strengthening of chemically similar species, which is potentially promising for determining the relevant application of MoP in heterogeneous catalysis.

Based on these previous interesting theoretical studies, we can easily find that they mainly focus on (001) surface with one Mo-termination and one P-termination, as well as (100) surface. However, experimentally, there are several peaks in the XRD profiles of MoP catalyst, such as (101), (100), (001), (110), (111) and (102). Among these surface orientations, the (101) surface was the most common one in all available XRD results [30–37]. In this respect, two primary but interesting issues of MoP catalyst arise, which cannot be ignored. Who is the most stable and representative surface of MoP? Which surface or surfaces will determine the catalytic properties of it? To answer these two questions, DFT based surface energy calculation can be used to identify the surface stability, while mechanism calculation can reveal the activity difference of each surface. In this work, we focused on the first question and performed a systematic DFT calculation of MoP surface energies. Wulff construction was also used to build the equilibrium particle shape of the MoP catalyst. In addition, atomistic thermodynamic method was applied to explain the changed stabilities of MoP surfaces with experimental conditions. Our goal is to offer a rational model for further theoretical mechanism study and have a more comprehensive understanding of the MoP system.

2. Computational details

2.1. Methods

All calculations were based on DFT method by using the Vienna Ab initio Simulation Package (VASP) [38,39]. The projected augmented wave method (PAW)[40] was applied and the electron exchange and correlation energies were calculated within the generalized gradient approximation with the Perdew-Burke-Ernzerhof (GGA-PBE) functional [41,42]. The optimization of structures was done when the force tolerance was lower than 0.01 eV/Å and the energy difference was lower than 10^{-5} eV. The cutoff energy was set as 400 eV. Spin-polarization was also included throughout our calculations.

2.2. Models

The XRD data of MoP [43] showed that it had WC-type structure and belonged to P6(−)m2 space group with lattice parameters of a = b = 3.223 Å and c = 3.191 Å. Several studies reported MoP including WC-, NaCl-, and zinc-blende (ZB)-type structures also showed that WC-type structure was most stable [44,45]. We therefore used the WC-type structure as our model in this work. For bulk optimization, a 15 × 15 × 15 Monkhorst-Pack k-point grid was used for sampling the Brillouin zone, and the identified lattice parameters (a = b = 3.239 Å, c = 3.193 Å) agreed well with the experimental values [43]. For the surface energy calculations, we chose the periodic slab models with 15 Å vacuum layer and 21–34 Å thickness, the detailed structural information of them were given in supplementary information (Table S1).

3. Result and discussion

3.1. Methods for calculating surface energies

For MoP system, eight facets with 22 different terminations were chosen as our models, which were widely identified by available experimental XRD profiles. Most importantly, they include both low Miller index (001), (100), (101), (110) and (111) surfaces as well as high Miller index (102), (112) and (201) surfaces, which are without the scope of previous theoretical investigations. Interestingly, these eight surfaces have very special surface structures, and can be divided into three groups.

For example, the first group includes (110) and (112) surfaces, which have only one mixed Mo/P termination exposing both Mo and P atoms, and can form stoichiometric as well as symmetric slabs by cleavage (Fig. 1a). The second group includes (001) and (111) surfaces, which have two different terminations and each of them can form symmetric but non-stoichiometric slabs by cleavage (Fig. 1(b–d)). Actually, these two groups are the commonly known surface structures. However, the third group that includes (100), (101), (102) and (201) surfaces are very special. They have four different terminations, but none of them can form symmetric slabs by cleavage (Fig. 1 (e–h)). Taking the (100) surface as an example, the T1′ and T2′ terminations are both Mo-terminated, but the distance between the first surface layer and the second surface layer ($d_{12'}$ and $d_{23'}$) are different (Fig. 1g), so they are actually different. Similarly, the T3′ and T4′ terminations are both P-terminated, but they also have different interlayer distances (Fig. 1h). The detailed surface structures of these eight surfaces with 22 terminations are shown in Fig. S1. Clearly, these three groups of surface terminations arise new questions for the calculations of their surface energies, especially for the third group of asymmetric surface terminations. We therefore show the detailed method for acquiring the surface energies of these three groups of MoP surfaces.

3.1.1. symmetric and stoichiometric termination

For the symmetric and stoichiometric termination as shown in Fig. 1a, it is the most common and easiest situation for surface energy calculation, which can be calculated by normal method with the following equation:

$$\gamma = (E_{total} - nE_{bulk})/2A \quad (1)$$

Where γ is the surface energy of MoP facet, E_{total} is the total energy of the relaxed MoP surface slab, E_{bulk} is the total energy of MoP bulk unit cell, n is the number of the bulk MoP unit in this slab, and A is the surface area of the slab model.

However, this normal method does not work for the symmetric/non-stoichiometric, asymmetric/stoichiometric as well as asymmetric/non-stoichiometric terminations. Therefore, a new methodology for calculating surface energies of these special terminations are highly desired. Fortunately, we found an easy and useful way for those situations.

3.1.2. symmetric and non-stoichiometric termination

From a point view of physics, the surface energy is consisted of the cleavage energy (E_{cle}) and the relaxation energy (E_{rel}) [46–48], and the surface energy is generally a sum of E_{cle} and E_{rel}.

$$\gamma = (E_{cle} + E_{rel})/A \quad (2)$$

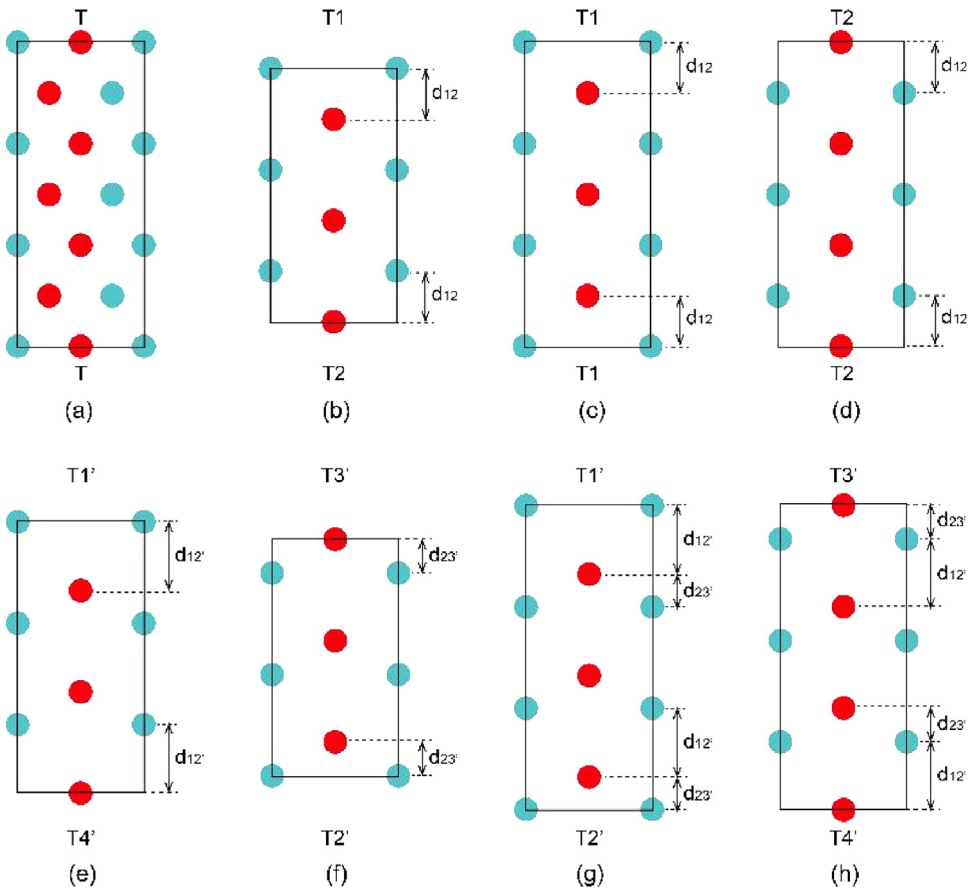

Fig. 1. Schematic side views of three groups of MoP(*hkl*) surfaces with different structure properties: (a) one termination, stoichiometric and symmetric; (b–d) two terminations, non-stoichiometric and symmetric; (e–h) four terminations, non-stoichiometric and asymmetric.

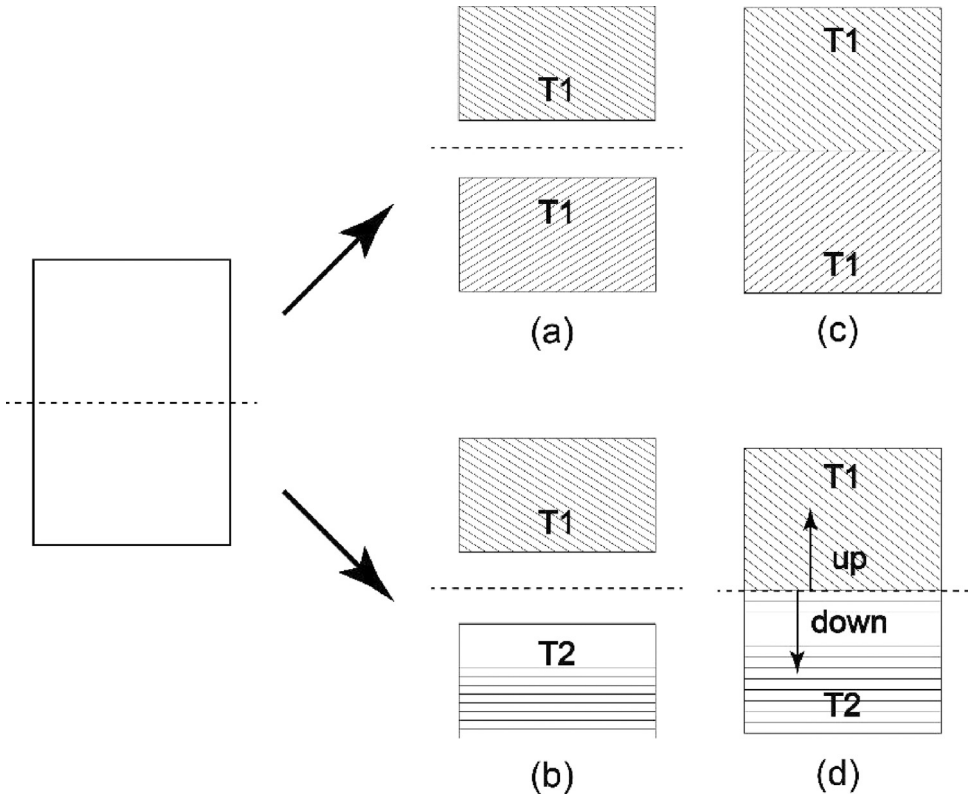

Fig. 2. Schematic view of cleavage energies (E_{cle}) of two same (a) and different (b) terminations as well as relaxation energies(E_{rel}) of symmetric (c) and asymmetric (d) slabs.

When cleaving the bulk MoP, two terminations are generated simultaneously, and the cleavage energy is divided equally between them. Furthermore, the electronic effect due to the broken of the heteroatom-bond can be ignored because of the similar electronegativity of P and Mo (2.19 and 2.16, respectively) [49]. Consequently, the cleavage energies of two generated terminations (either they are the same (Fig. 2a) or different (Fig. 2b)) from one cleavage are supposed to be equal. Therefore, the cleavage energy of a stoichiometric slab can be obtained from the following equation:

$$E_{cle} = (E_{unrelax} - nE_{bulk})/2 \quad (3)$$

$E_{unrelax}$ is the total energy of the unrelaxed MoP surface slab.

For a symmetric slab (Fig. 2c), E_{rel} can be easily obtained from the equation:

$$E_{rel} = (E_{total} - E_{unrelax})/2 \quad (4)$$

Therefore, for symmetric and non-stoichiometric slab as shown in Fig. 1(b–d), we can directly use Eq. (2)–(4), to get the surface energy of each termination. For example, the asymmetric and stoichiometric model (Fig. 1b) can be used to calculate the cleavage energy of T1 and T2 by Eq. (3). Then, the symmetric and non-stoichiometric models (Fig. 1c and d) can be applied to calculate the relaxation energies of T1 and T2 terminations by Eq. (4), respectively. Finally, the surface energies of T1 and T2 can be acquired by using Eq. (2).

3.1.3. Asymmetric and stoichiometric/non-stoichiometric terminations

For asymmetric slabs (Fig. 1(e–h)), the stoichiometric slab in Fig. 1e can be used to calculate the cleavage energy of T1′ and T4′ terminations by Eq. (3), because the cleavage here can generate T1′ and T4′ simultaneously. Similarly, the stoichiometric slab in Fig. 1f can be used to calculate the cleavage energy of T2′ and T3′ terminations by Eq. (3).

For these asymmetric slabs, however, the relaxation energy of up and down termination cannot be easily calculated from Eq. (4), which should be treated individually.

As shown in Fig. 2d, the slab can be divided into two parts from the middle. Then the relaxation energy of T1 or T2 termination can be obtained from the following equations:

$$E_{rel}(T1) = E_{T1\text{-}relax} - E_{unrelax} \quad (5)$$

$$E_{rel}(T2) = E_{T2\text{-}relax} - E_{unrelax} \quad (6)$$

$E_{T1\text{-}relax}$ is the energy of the slab only with the up-half part relaxed, $E_{T2\text{-}relax}$ is the energy of the slab only with the down half part relaxed. However, in this case, the relaxed part should be thick enough to avoid the errors, and the detailed test results were given in supplementary information (Table S2). On the basis of the calculated relaxation energy and cleavage energy of each termination (Supplementary Table S3), the surface energies of them could be acquired by using Eq. (2).

Based on the method for different situations, we finally obtain the surface energies of each termination, which are listed in Table 1. It is found that the Mo-termination has lower surface energy than P-termination for the (001) (111) and (100) surfaces. If the most stable termination of each surface is chosen for comparison, the surface stability follows the order of (101)-T1 > (100)-T2 > (112) > (201)-T2 > (111)-Mo > (102)-T1 > (110) > (001)-Mo. Among all the terminations, the T1-terminated (101) surface exposing both Mo and P atoms has the lowest surface energy of 1.83 J/m^2 and is therefore the most stable termination of MoP catalyst.

However, the surface stability and the calculated values are quite different from the previous DFT study by Yue et al. [14], where the Mo-terminated surfaces were found to have higher surface energies than P-terminated surfaces, and the (001)-P termination has the lowest surface energy of 2.63 J/m^2. Actually, this large difference is caused by several points. At first, Yue et al. [14] only got the total surface energy of two different terminations rather than the exact value for each individual termination. Secondly, they used a very general equation ($\gamma = [E_{(slab)} - n_{Mo}\mu_{Mo} - n_P\mu_P]/A$) for surface energy calculation, and the chemical potential of Mo (μ_{Mo}) and P (μ_P) were set to be −11.818 and −5.851 eV, respectively. However, there was no information about how they got these two values. For comparison, Table 1 also listed our calculated value with the equations in the work from Yue et al., [14] and the obtained values were very similar to theirs. In addition, Kibsgaard et al. [50] suggested that the (001) surface was among the top 3–5 most likely surfaces by using the Bravais-Friedel-Donnay-Harker (BFDH) [51] crystal morphology algorithm, which was only based on geometry without any energetic information in identifying the exact stability of each surface termination. Therefore, further analysis was performed to validate our method.

Table 1
The calculated surface energies (γ) of different terminations of MoP(*hkl*) surfaces and comparison with the reference.

(*hkl*)	γ(J/m^2)	Ref. [14] (a)	(*hkl*)	γ (J/m^2)	Ref. [14]
(110)	2.39		(101)-T2	3.05	
(112)	2.04		(101)-T3	3.39	
(001)-Mo	2.56	7.88 (7.96)	(101)-T4	2.01	3.54 (3.56)
(001)-P	2.94	2.63 (3.29)	(102)-T1	2.20	
(111)-Mo	2.19		(102)-T2	2.40	
(111)-P	2.48		(102)-T3	2.46	
(100)-T1 (Mo)	3.69	8.16 (8.18)	(102)-T4	2.48	
(100)-T2 (Mo)	1.93		(201)-T1	2.80	
(100)-T3 (P)	2.28	3.88 (3.92)	(201)-T2	2.05	
(100)-T4 (P)	4.02		(201)-T3	2.10	
(101)-T1	1.83	6.87 (6.92)	(201)-T4	2.92	

(a) the value in parenthesis is obtained by using the energy of the surface slab in this work and the equation in ref [14].

3.2. Morphology of MoP catalyst

On the basis of the calculated surface energies in Table 1, Wulff construction [52] was performed to describe the ideal morphology of MoP catalyst. In general, the Wulff construction is a method to determine the equilibrium shape of a droplet or crystal of fixed volume, and it provides an ideal shape of the catalyst morphology. As shown in Fig. 3, under ideal vacuum condition, only six of the eight calculated surfaces expose on Wulff shape, and the (101) surface has the largest contribution of 36.2%, followed by (112) surface (24.1%), (100) surface (19.3%), (111) surface (12.3%), (110) surface (4.3%) and (102) surface (3.8%).

In this respect, our simulated results clearly reveal that the (101) surface is the most stable and also the highly exposed surface on Wulff particle, which indicates its representative and important

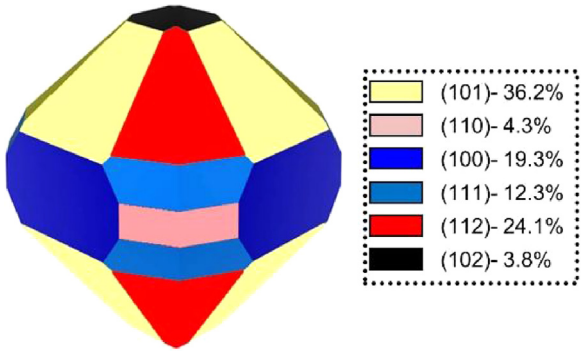

Fig. 3. Wulff particle of MoP at ideal condition.

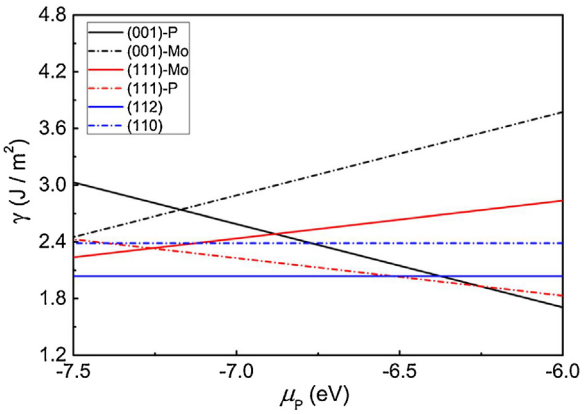

Fig. 4. Relationship between surface energy (γ) and chemical potential of P (μ_P).

role in determining the properties of MoP catalyst. Actually, this finding is consistent with the previous experimental studies, where the (101) surface is found to have the most intensive XRD signal [14,30–34]. In addition, the (101) and (100) surfaces were both detected by TEM measurement [36], which were also the most and second most stable surfaces in our theoretical calculations. However, available experimental references [30,35,36] also detected the existence of (001) surface, which was the least stable one in Table 1 and didn't expose on the Wulff particle in Fig. 3. It should be noted that the surface stability would change with experimental conditions, which could be shown with thermodynamics analysis.

3.3. Surface stability and experimental condition

In this part, we applied *ab initio* atomistic thermodynamic method [53–57] to check the effects of experimental conditions on the stabilities of different terminations, where P chemical potential (μ_P) was used to describe the changes in temperature and gas phase pressures. The detailed description of this method could be found in the supplementary information. In brief, the changes in experimental conditions result in the changes in the value of μ_P, and the surface energy of MoP termination is a function of μ_P:

$$\gamma(T,p) = [E_{\mathrm{MoP}[hkl]} - n_{\mathrm{Mo}}E_{\mathrm{bulk}} + (n_{\mathrm{Mo}} - n_{\mathrm{P}})\mu_{\mathrm{P}}]/2A \quad (7)$$

where $E_{\mathrm{MoP}[hkl]}$ and E_{bulk} are the electronic energies of MoP[*hkl*] surface and MoP bulk, which can be calculated by VASP. n_{Mo} and n_{P} are the numbers of Mo and P atoms in the slab, A is the area of the slab.

However, this method could only work for the symmetric (112), (110), (001) and (111) surfaces. As shown in Fig. 4, the surface energies of each termination have different changes with μ_P. For example, the surface energies of Mo terminations such as (001)-Mo and (111)-Mo have positive slops with μ_P, while those P terminations have negative slops. There is also a clear change in the stability orders of different surfaces with μ_P. Clearly, the (001)-P termination will become most stable at high P chemical potential (i.e., $\mu_P = -6.0$ eV corresponding to T = 925 K and $PH_3/H_2 = 1/1000$). Actually, this also explained the differences in the experimentally detected surfaces from different references, i.e. only (101) and (100) surface were detected by some references while (001) was detected by others. Obviously, our simulated results agree very well with experimental findings, which finally validate our method for surface energy calculations.

4. Conclusion

Based on the concepts of cleavage energy and relaxation energy as well as the density functional theory calculations, a useful method was introduced to calculate the surface energies of asymmetric and non-stoichiometric surface terminations of MoP catalyst. It is found that the T1-terminated (101) surface with both exposed Mo and P atoms has the lowest surface energy, followed by the (100) surface. Wulff construction shows that only six of the eight calculated surfaces could expose at ideal condition, and the (101) surface has the largest contribution. These results are supported by available XRD and TEM measurements, which strongly validate our methodology.

Ab initio atomistic thermodynamic method was applied to study the relative stability of symmetric MoP surfaces under different preparation conditions. A relationship between MoP surface energies and the preparation conditions (T, *p* and gas mixture) was built through P chemical potential (μ_P). Taking PH_3/H_2 as phosphorus source, it is found that the (001)-P termination become the most stable at high P chemical potential. This manner also rationalized the experimentally detected different surfaces with distinguish preparation conditions.

In summary, the reported method here for surface energy calculation could be extended to other similar systems with asymmetric surface terminations. Our results also provide important references for selecting a rational surface for further reaction mechanism calculations on MoP catalyst. The high stability and exposure of (101) surface indicates that special attention should be paid on this facet for further mechanism investigations. The studies of catalytic activities on several MoP surfaces are our ongoing interests and will be discussed elsewhere.

Acknowledgments

This work was supported by the National Natural Science Foundation of China (no. U1510103). The calculations were performed using supercomputers at the Supercomputing Center of Shanxi University.

References

[1] S. Zaman, K.J. Smith, A review of molybdenum catalysts for synthesis gas conversion to alcohols: catalysts, mechanisms and kinetics, Cat. Rev. Sci. Eng. 54 (2012) 41–132.
[2] A. Malinowski, Application of Molybdenum Catalysts in Biorefinery Materials and Processes for Energy: Communicating Current Research and Technological Developments, A. Méndez-Vilas, Badajoz, 2013, pp. 206–211.
[3] J.A. Botas, D.P. Serrano, A. Garcia, J.De Vincente, R. Ramos, Catalytic conversion of rapeseed oil into raw chemicals and fuels over Ni- and Mo-modified nanocrystalline zsm-5 zeolite, Catal. Today 195 (2012) 59–70.
[4] S.T. Oyama, Novel catalysts for advanced hydroprocessing: transition metal phosphides, J. Catal. 216 (2003) 343–352.
[5] J. Kibsgaard, T.F. Jaramillo, Molybdenum phosphosulfide: an active acid-stable, earth-abundant catalyst for the hydrogen evolution reaction, Angew. Chem. Int. Ed. 53 (2014) 14433–14437.
[6] P. Xiao, W. Chen, X. Wang, A review of phosphide-based materials for electrocatalytic hydrogen evolution, Adv. Energy Mater. 5 (2015) 1500985.
[7] X. Zou, Y. Zhang, Noble metal-free hydrogen evolution catalysts for water splitting, Chem. Soc. Rev. 44 (2015) 5148–5180.
[8] S. Izhar, M. Nagai, Transition metal phosphide catalysts for hydrogen oxidation reaction, Catal. Today 146 (2009) 172–176.
[9] C. Stinner, R. Prins, T. Weber, Formation structure, and HDN activity of unsupported molybdenum phosphide, J. Catal. 191 (2000) 438–444.
[10] J. Bai, X. Li, A. Wang, R. Prins, Y. Wang, Hydrodesulfurization of dibenzothiophene and its hydrogenated intermediates over bulk MoP, J. Catal. 287 (2012) 161–169.
[11] J.X. Chen, H. Shi, L. Li, K.L. Li, Deoxygenation of methyl laurate as a model compound to hydrocarbons on transition metal phosphide catalysts, Appl. Catal. B: Environ. 144 (2014) 870–884.
[12] Q. Guo, L. Ren, Hydrodechlorination of trichloroethylene over MoP/gamma-Al_2O_3 catalyst with high surface area, Catal. Today 264 (2016) 158–162.
[13] P. Liu, W.T. Chang, J. Wang, M.Y. Wu, Y.X. Li, MoP/H beta catalyst prepared by low-temperature auto-combustion for ydroisomerization of n-heptane, Catal. Commun. 66 (2015) 79–82.
[14] Q.D. Yue, Y.Y. Wan, Z.J. Sun, X.J. Wu, Y.P. Yuan, P.W. Du, MoP is a novel, noble-metal-free cocatalyst for enhanced photocatalytic hydrogen production from water under visible light, J. Mater. Chem. A 3 (2015) 16941–16947.

[15] X. Wang, P. Sun, J. Qin, J. Wang, Y. Xiao, M. Cao, A three-dimensional porous MoP@C hybrid as a high-capacity, long-cycle life anode material for lithium-ion batteries, Nanoscale 8 (2016) 10330–10338.
[16] S.F. Zaman, K.J. Smith, Synthesis gas conversion over MoP catalysts, Catal. Commun. 10 (2009) 468–471.
[17] S.F. Zaman, K.J. Smith, A study of K-promoted MoP–SiO_2 catalysts for synthesis gas conversion, Appl. Catal. A 378 (2010) 59–68.
[18] Z. Feng, C. Liang, W. Wu, Z. Wu, R.A. van Santen, C. Li, Carbon monoxide adsorption on molybdenum phosphides: fourier transform infrared spectroscopic and density functional theory studies, J. Phys. Chem. B 107 (2003) 13698–13702.
[19] P. Liu, J.A. Rodriguez, Catalytic properties of molybdenum carbide, nitride and phosphide: a theoretical study, Catal. Lett. 91 (2003) 247–252.
[20] S.F. Zaman, M. Daous, L. Petrov, A DFT study of CO adsorption and dissociation over MoP(001) plane, Comptes Rendus De Lacadeímie Bulgare Des Sciences 66 (2013) 1535–1540.
[21] S.F. Zaman, M. Daous, L. Petrov, A DFT study of CO adsorption and dissociation over MoP(100) plane, Comptes Rendus De Lacadeímie Bulgare Des Sciences 67 (2014) 1083–1090.
[22] S.F. Zaman, M. Daous, L. Petrov, Dissociative adsorption of hydrogen on MoP (100) plane: a DFT study, Comptes Rendus De Lacadeímie Bulgare Des Sciences 68 (2015) 1503–1510.
[23] S.F. Zaman, M. Daous, L. Petrov, A DFT study of hydrogen dissociation over MoP (001) plane, Comptes Rendus De Lacadeímie Bulgare Des Sciences 67 (2014) 777–782.
[24] V. Milman, B. Winkler, R. Gomperts, Molybdenum phosphide as an o-propylaniline hydrodenitrogenation catalyst: a first principles study, Chem. Eur. J. 10 (2004) 6279–6284.
[25] Y. Li, W. Guo, H. Zhu, L. Zhao, M. Li, S. Li, D. Fu, X. Lu, H. Shan, Initial hydrogenations of pyridine on MoP(001): a density functional study, Langmuir 28 (2012) 3129–3137.
[26] Z. Deng, Y. Lei, X. Lu, W. Wang, H. Zhu, S. Ng, W. Guo, C.L. Wu, Hydrodenitrogenation of pyridine on MoP(010): competition between hydrogenation and denitrification, Inorg. Chim. Acta 435 (2015) 30–37.
[27] S.R. Li, X.Q. Lu, H.Y. Zhu, W.Y. Guo, Mechanism of C-N bond cleavage in aniline on MoP(001) surface, Acta Phys.-Chim. Sin. 32 (2016) 465–473.
[28] J. Ren, C.F. Huo, X.D. Wen, Z. Cao, J. Wang, Y.W. Li, H. Jiao, Thiophene adsorption and activation on MoP(001), γ-Mo_2N(100), and Ni_2P(001): density functional theory studies, J. Phys. Chem. B 110 (2006) 22563–22569.
[29] M. Fields, C. Tsai, L.D. Chen, F. Abild-Pedersen, J.K. Nørskov, K. Chan, Scaling relations for adsorption energies on doped molybdenum phosphide surfaces, ACS Catal. 7 (2017) 2528–2534.
[30] A. Montesinos-Castellanos, E. Lima, A. Vázquez-Zavala, J.A.de los Reyes, M.A., Vera, Industrial alumina as a support of MoP: catalylic activity in the hydrodesulfurization of dibenzothiophene, Vera Revista Mexicana de Ingeniería Química 11 (2012) 105–120.
[31] R. Cheng, Y. Shu, L. Li, J. Sun, X. Wang, T. Zhang, CO adsorption on highly dispersed MoP/Al_2O_3 prepared with citric acid, Thermochim. Acta 450 (2006) 42–46.
[32] F. Li, Z. Zhao, Q. Li, T. Zhao, C. Li, G. Sun, Effect of reduction temperature on hydrofining performance of supported molybdenum phosphide catalyst, J. Nat. Gas Chem. 14 (2005) 233–237.
[33] I.I. Abu, K.J. Smith, The effect of cobalt addition to bulk MoP and Ni_2P catalysts for the hydrodesulfurization of 4,6-dimethyldibenzothiophene, J. Catal. 241 (2006) 356–366.
[34] Z.W. Yao, L. Wang, H. Dong, A new approach to the synthesis of molybdenum phosphide via internal oxidation and reduction route, J. Alloy. Compd. 473 (2009) L10–L12.
[35] P. Xiao, M.A. Sk, L. Thia, X. Ge, R.J. Lim, J.Y. Wang, K.H. Lim, X. Wang, Molybdenum phosphide as an efficient electrocatalyst for the hydrogen evolution reaction, Energy Environ. Sci. 7 (2014) 2624–2629.
[36] D.C. Phillips, S.J. Sawhill, R. Self, M.E. Bussell, Synthesis characterization, and hydrodesulfurization properties of silica-supported molybdenum phosphide catalysts, J. Catal. 207 (2002) 266–273.
[37] Y. Teng, A. Wang, X. Li, J. Xie, Y. Wang, Y. Hu, Preparation of high-performance MoP hydrodesulfurization catalysts via a sulfidation-reduction procedure, J. Catal. 266 (2009) 369–379.
[38] G. Kresse, J. Furthmüller, Efficiency of ab-initio total energy calculations for metals and semiconductors using a plane-wave basis set, Comput. Mater. Sci. 6 (1996) 15–50.
[39] G. Kresse, J. Furthmüller, Efficient iterative schemes for *ab initio* total-energy calculations using a plane-wave basis set, Phys. Rev. B 54 (1996) 11169–11186.
[40] P.E. Blöchl, Projector augmented-wave method, Phys. Rev. B 50 (1994) 17953–17979.
[41] J.P. Perdew, K. Burke, M. Ernzerhof, Generalized gradient approximation made simple, Phys. Rev. Lett. 77 (1996) 3865–3868.
[42] J.P. Perdew, K. Burke, M. Ernzerhof, Errata: generalized gradient approximation made simple, Phys. Rev. Lett. 78 (1997) 1396–1397.
[43] S. Rundqvist, T. Lundström, X-ray studies of molybdenum and tungsten phosphides, Acta Chem. Scand. 17 (1963) 37–46.
[44] P. Pandit, S.P. Sanyal, Structural stability and electronic properties of MoP, AIP Conf. Proc. 1349 (2011) 855–856.
[45] P. Pandit, S.P. Sanyal, Lattice dynamics and elastic properties of MoP, AIP Conf. Proc. 1447 (2012) 845–846.
[46] J.M. Zhang, Q. Pang, K.W. Xu, V. Ji, First-principles study of the (001) surface of cubic $PbTiO_3$, Surf. Interface Anal. 40 (2008) 1382–1387.
[47] R.I. Eglitis, Ab initio hybrid DFT calculations of $BaTiO_3$, $PbTiO_3$ $SrZrO_3$ and $PbZrO_3$ (111) surfaces, Appl. Surf. Sci. 358 (2015) 556–562.
[48] Y. Takagi, T. Yamada, M. Yoshino, T. Nagasaki, Ab initio study on face azimuth dependency of surface energy and structure in $PbTiO_3$, Ferroelectrics 490 (2016) 167–173.
[49] A.L. Allred, Electronegativity values from thermochemical data, J. Inorg. Nucl. Chem. 17 (1961) 215–221.
[50] J. Kibsgaard, C. Tsai, K. Chan, J.D. Benck, J.K. Nørskov, F. Abild-Pedersen, T.F. Jaramillo, Designing an improved transition metal phosphide catalyst for hydrogen evolution using experimental and theoretical trends, Energy Environ. Sci. 8 (2015) 3022–3029.
[51] R. Docherty, K.J. Roberts, P. Bennema, G. Clydesdale, Application of Bravais-Friedel-Donnay-Harker, attachment energy and Ising models to predicting and understanding the morphology of molecular crystals, J. Phys. D: Appl. Phys. 24 (1991) 89–99.
[52] G.Z. Wulff, Zur Frage der Geschwindigkeit des Wachstums und der Auflösung der Krystallflächen, Kristallogr. 34 (1901) 449–530.
[53] K. Reuter, M. Scheffler, Composition, structure, and stability of RuO_2(110) as a function of oxygen pressure, Phys. Rev. B 65 (2001) 035406.
[54] T. Wang, X.W. Liu, S.G. Wang, C.F. Huo, Y.-W. Li, J. Wang, H. Jiao, Stability of β-Mo_2C facets from ab initio atomistic thermodynamics, J. Phys. Chem. C 115 (2011) 22360–22368.
[55] T. Wang, Q.Q. Luo, Y.-W. Li, J. Wang, M. Beller, H. Jiao, Stable surface terminations of orthorhombic Mo_2C catalysts and their co activation mechanisms, Appl. Catal. A 478 (2014) 146–156.
[56] T. Wang, Y.-W. Li, J. Wang, M. Beller, H. Jiao, Dissociative hydrogen adsorption on the hexagonal Mo_2C phase at high coverage, J. Phys. Chem. C 118 (2014) 8079–8089.
[57] T. Wang, X. Tian, Y.-W. Li, J. Wang, M. Beller, H. Jiao, Coverage-dependent CO adsorption and dissociation mechanisms on iron surfaces from DFT computations, ACS Catal. 4 (2014) 1991–2005.